

# Influence of the porous structure and functionality of the MIL type metal-organic frameworks and carbon matrices on the adsorption of 2,4-dichlorophenoxyacetic acid

V. I. Isaeva,<sup>a\*</sup> S. A. Kulaishin,<sup>a</sup> M. D. Vedenyapina,<sup>a</sup> V. V. Chernyshev,<sup>b,c</sup> G. I. Kapustin,<sup>a</sup>  
V. V. Vergun,<sup>a</sup> and L. M. Kustov<sup>a</sup>

<sup>a</sup>N. D. Zelinsky Institute of Organic Chemistry, Russian Academy of Sciences,  
47 Leninsky prospekt, 119991 Moscow, Russian Federation,

E-mail: sharf@ioc.ac.ru

<sup>b</sup>A. N. Frumkin Institute of Physical Chemistry and Electrochemistry, Russian Academy of Sciences,  
31 Leninsky prospekt, 119071 Moscow, Russian Federation

<sup>c</sup>Department of Chemistry, M. V. Lomonosov Moscow State University,  
1-3 Leninskie Gory, 119991 Moscow, Russian Federation

The adsorption of 2,4-dichlorophenoxyacetic acid (2,4-D) from aqueous solutions on different porous materials was studied. The materials included micro- and mesoporous carbon matrices of different genesis and metal-organic frameworks (MOFs) of the MIL type such as microporous matrices MIL-53(Al) ( $\text{AlOHbdc}$ , bdc = benzene-1,4-dicarboxylate) and  $\text{NH}_2\text{-MIL-53(Al)}$  ( $\text{AlOHbdc}$ , abdc = 2-aminobenzene-1,4-dicarboxylate), as well as mesoporous matrix  $\text{NH}_2\text{-MIL-101(Al)}$  ( $\text{Al}_3\text{O(abdc)}_3$ ). It is found that the efficiency of liquid phase adsorption is affected by the texture and functionality of the studied materials, whereas in the case of MOFs, the adsorption efficiency is also under the influence the framework flexibility. The MOF materials and mesoporous carbon matrices show a higher adsorption rate than microporous carbon matrices. The flexible microporous MIL-53(Al) framework and microporous coconut shell activated carbon (CSAC) exhibit the highest adsorption capacity with respect to 2,4-D.

**Key words:** kinetics, adsorption from aqueous medium, herbicide, activated carbons, metal-organic frameworks (MOFs).

Currently, a serious threat to the environment is posed by the pollution of ground and surface waters with toxic compounds such as dyes, herbicides, and drugs.<sup>1,2</sup> Herbicides are generally resistant to commonly used treatment methods such as UV irradiation,<sup>3</sup> coagulation,<sup>4</sup> flocculation or ultrafiltration,<sup>5</sup> and biodegradation.<sup>6</sup> Liquid-phase adsorption represents an alternative method for removing herbicides from aqueous media. Activated carbons,<sup>7</sup> fly ash,<sup>8</sup> zeolites,<sup>9</sup> and mesoporous silicates<sup>10</sup> are used as porous adsorbents. In particular, activated carbons of various origins are widely used for the adsorption of physiologically active organic compounds (e.g., herbicides) from wastewater.<sup>5</sup>

Carbon matrices are actively used as adsorbents because of their strong interaction with organic compounds dissolved in water.<sup>11</sup> It is known that textural characteristics such as the size and shape of pores,<sup>12</sup> as well as the presence of specific adsorption sites<sup>13</sup> determine the efficiency of adsorption.

Metal-organic frameworks (MOFs) being hybrid nanoporous materials are the most promising for the adsorption removal of toxic compounds from water.<sup>14–18</sup> MOFs are crystalline porous coordination polymers possessing a three-

dimensional structure formed by metal ions and organic molecules (linkers).<sup>19</sup>

The successful application of MOF matrices to the effective removal of toxic compounds from aqueous phases is related to their developed surfaces and high porosity, the ability to purposefully control the shape and size of pores in the micro- and meso-ranges, as well as the chemical properties of pore surfaces.<sup>20,21</sup> The design of the MOF materials for selective adsorption consists in formation of coordinatively unsaturated sites<sup>22</sup> and modification of their intracrystalline space with specific molecules or particles.<sup>11,23</sup>

Organic compounds present in wastewater can be adsorbed by MOF matrices, first of all, due to electrostatic interactions and  $\pi$ – $\pi$  stacking that is an interaction between aromatic moieties of molecules of adsorbate and linkers in the MOF framework.<sup>1,20,24,25</sup> The adsorption is facilitated by the increase in the pore size under the action of an external influence, a phenomenon known to MOFs as the breathing effect.<sup>1</sup>

In particular, it was found that the electrostatic interactions between the adsorbent and adsorbate and the

flexibility of framework of "breathing" matrices of some MOFs such as MIL-53(Cr) and MIL-53(Al)<sup>26</sup> are important factors determining the efficiency of adsorption of organic compounds.<sup>1,25,27</sup>

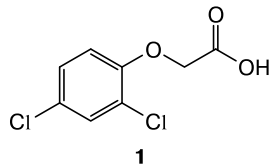
The present study is devoted to the investigation of the role of the porous structure and composition of adsorbents in adsorption of the herbicide 2,4-dichlorophenoxyacetic acid (2,4-D) from the aqueous medium. Two types of adsorbents were chosen for this study. Those are micro- and mesoporous carbon matrices with different textural characteristics and functional groups on the surface and MOF matrices with different porous structures, compositions, and framework flexibilities. Comparison of the efficiencies of the above adsorbents is important for understanding the mechanisms of adsorption on the adsorbents of different nature and, therefore, for the targeted development of adsorbents with desired properties.

## Experimental

The microporous frameworks MIL-53(Al) ( $\text{AlOH}_{\text{bdc}}$ , bdc = benzene-1,4-dicarboxylate and  $\text{NH}_2\text{-MIL-53(Al)}$  ( $\text{AlOH}_{\text{abdc}}$ , abdc = 2-aminobenzene-1,4-dicarboxylate), and the mesoporous structure  $\text{NH}_2\text{-MIL-101(Al)}$  ( $\text{Al}_3\text{O}(\text{abdc})_3$ ) were included in this study.

The following carbon adsorbents were used: coconut shell activated carbon (CSAC) (Pingluo Derun Charcoal Carbon Co., Ltd., Germany),<sup>28</sup> samples based on polyvinyl chloride (PVC), which were prepared according to a known procedure<sup>29</sup> by carbonization and activation in  $\text{CO}_2$  or Ar flow at different heating rates, and a synthetic carbon material representing a composite of Sibunite (pilot production of the Siberian Branch of the Russian Academy of Sciences, Novosibirsk, Russian Federation), a pyrolytic carbon modification, and soot.<sup>30</sup>

Commercially available reagents obtained from Acros were used without additional purification. *N,N'*-Dimethylformamide (DMF) used as a solvent was purified by distillation over  $\text{CaH}_2$  under reduced pressure. Adsorption was studied using 2,4-dichlorophenoxyacetic acid **1** (2,4-D) of >98% purity obtained from Sigma-Aldrich.



**Synthesis of MIL-53(Al).** The sample was prepared with the use of microwave radiation according to the known procedure,<sup>31</sup> which, however, was somewhat modified by changing the solvent system. The starting reagents, *viz.*,  $\text{AlCl}_3 \cdot 6\text{H}_2\text{O}$  (1.21 g, 5.01 mmol), benzene-1,4-dicarboxylic acid (0.42 g, 2.53 mmol), and a mixture of solvents (0.5 mL of deionized water and 5.5 mL of DMF), were mixed in a glass ampoule and heated under atmospheric pressure in the chamber of a Vigor microwave oven (RF) (200 W, 125 °C) for 30 min. The obtained sample of MIL-53(Al) was separated by centrifugation and washed with DMF (3×20 mL) and distilled water (3×30 mL). The matrix was

calcined at 330 °C for 72 h in air and then additionally heated at 440 °C for 3 h to completely remove residues of benzene-1,4-dicarboxylic acid from the pores of the framework.

**Synthesis of  $\text{NH}_2\text{-MIL-53(Al)}$ .** The sample was prepared by microwave activation of the reaction mixture containing 2-amino-benzene-1,4-dicarboxylic acid instead of benzene-1,4-dicarboxylic acid. The initial reagents, *viz.*,  $\text{AlCl}_3 \cdot 6\text{H}_2\text{O}$  (3.94 g, 16 mmol), 2-aminobenzene-1,4-dicarboxylic acid (3.01 g, 15 mmol), and a mixture of solvents (20 mL of deionized water and 20 mL of DMF), were placed into a glass ampoule and heated under atmospheric pressure in the chamber of a Vigor microwave oven (200 W, 130 °C) for 15 min. The light-yellow precipitate was separated by centrifugation and washed with DMF (3S20 mL) and distilled water (3S30 mL). The obtained sample of  $\text{NH}_2\text{-MIL-53(Al)}$  was heated in boiling DMF for 12 h, washed with water, and activated using a thermal vacuum treatment ( $10^{-3}$  Torr, 150 °C) for 4 h.

**Synthesis of  $\text{NH}_2\text{-MIL-101(Al)}$ .** The sample was prepared using microwave radiation under atmospheric pressure.<sup>31</sup> The starting reagents, *viz.*,  $\text{AlCl}_3 \cdot 6\text{H}_2\text{O}$  (0.51 g), 2-aminobenzene-1,4-dicarboxylic acid (0.56 g), and DMF (40 mL), were placed into a glass ampoule and heated under atmospheric pressure in the chamber of a Vigor microwave oven (200 W, 130 °C) for 20 min. The formed yellow precipitate was separated by centrifugation and washed with DMF (3×10 mL) and acetone (3×10 mL). The crystalline product was heated in boiling methanol (20 mL) under stirring for 24 h, separated by centrifugation, and activated using a thermal vacuum treatment ( $10^{-3}$  Torr, 130 °C) for 7 h.

**Physicochemical studies of the MIL samples.** Prepared MIL samples and carbon matrices were characterized using powder X-ray diffraction (PXRD), FE-SEM, and DRIFTS and exploring low-temperature nitrogen adsorption.

The microstructure of the synthesized samples was studied using field emission scanning electron microscopy (FE-SEM) and field emission scanning transmission electron microscopy (FE-STEM) with the use of a Hitachi SU8000 electron microscope (Japan). The images were taken detecting secondary electrons at an accelerating voltage of 2 kV and a distance of 5–6 mm (for SEM images) or in the mode of light-field imaging (detection of passed electrons) at an accelerating voltage of 30 kV<sup>32</sup> (for STEM images). The morphology of the samples was investigated taking into account the correction for the surface effects of the conducting layer deposit. The X-ray measurements were carried out at room temperature using an EMPYREAN diffractometer (Panalytical, Netherlands) (Cu-K $\alpha$  radiation, a nickel filter, a X'Celetor line detector, the Bragg-Brentano geometry). The porous structure and surfaces of the prepared materials were characterized using adsorption apparatus ASAP 2020 (Micromeritics ASAP-2020-Plus, USA) on the basis of measurements of nitrogen adsorption by volumetry; the porous structure parameters were calculated by the Brunauer–Emmett–Teller (BET) equation. After outgassing of a sample at 150 °C in *vacuo*, the nitrogen adsorption was measured at –196 °C and relative vapor pressure ( $P/P_0$ ) within 0.01–0.99.

**Adsorption measurements.** Adsorption of 2,4-D from aqueous solutions of predetermined concentrations ( $C_0 = 25$ –200 mg L<sup>–1</sup>) was carried out in a conical bulb equipped with a reflux condenser under permanent stirring with a magnetic stirrer (150 rpm) at room temperature. The herbicide concentration in a solution during achieving the adsorption equilibrium ( $C_e$ ) was determined

using UV spectroscopy by measurements of an absorption at  $\lambda = 283$  nm with the use a Hitachi U-1900 spectrophotometer (Japan).<sup>28</sup>

## Results and Discussion

The porous structure of the microporous matrices MIL-53(Al) and NH<sub>2</sub>-MIL-53(Al), which are formed by the AlO<sub>4</sub>(OH)<sub>2</sub> octahedra and the 2-aminobenzene-1,4-dicarboxylate linkers, represents a system of one-dimensional (unidirectional) channels.<sup>33</sup> These frameworks exhibit a significant breathing effect in the form of dynamic transformations of their structures. The effect involves pore size tuning of the matrix to accommodate the adsorbate molecules without the loss of crystallinity and without breaking bonds.<sup>11,34,35</sup> Because of this effect, the size of the 1D pores in the MIL-53(Al) and NH<sub>2</sub>-MIL-53(Al) frameworks is sensitive to dimensions of the adsorbed guest molecule.

It is known that the MOF flexibility significantly depends on the nature of substituents in the organic linker.<sup>33</sup> The comparative analysis of structures with the amino-containing linkers (abdc) and without the NH<sub>2</sub> groups (bdc) was aimed at the determination of the effect of the amino group on the adsorption characteristics of MOFs in the process of removal of 2,4-D from aqueous medium.

The pore system of mesoporous NH<sub>2</sub>-MIL-101(Al) framework is formed by two quasispherical cages of 2.4 and 2.9 nm in size, which are accessible through windows with a diameter of 1.2 and 1.6 nm, respectively.<sup>36</sup> Therefore, to reveal the effects of the porous structure of frameworks and specific surfaces of matrixes, the NH<sub>2</sub>-MIL-53(Al) and NH<sub>2</sub>-MIL-101(Al) matrices with the same 2-aminobenzene-1,4-dicarboxylate linkers, but different textural characteristics were selected.

### Physicochemical characteristics of the MIL materials.

The analysis of images obtained using scanning electron microscopy (Fig. 1) showed that the samples of metal-organic frameworks of the MIL type prepared in microwave fields crystallize in the form of nanoparticles of

similar size and shape. The MIL-53(Al) sample was obtained as ellipsoidal crystallites with the average size of 200–300 nm (Fig. 1, a). The NH<sub>2</sub>-MIL-53(Al) sample crystallizes in the form of prisms with an average size of ~300 nm (Fig. 1, b), whereas the NH<sub>2</sub>-MIL-101(Al) adsorbent was prepared as octahedral crystallites of 50–100 nm in size (Fig. 1, c).

The powder XRD data obtained for the prepared MIL samples confirmed that their structures correspond to the MIL-53(Al), NH<sub>2</sub>-MIL-53(Al), and NH<sub>2</sub>-MIL-101(Al) metal-organic frameworks reported earlier.<sup>25,36–38</sup>

The X-ray powder diffraction patterns of the MIL-53(Al), NH<sub>2</sub>-MIL-53(Al), and NH<sub>2</sub>-MIL-101(Al) samples are shown in Figs 2 and 3.<sup>37</sup> It is seen that the diffraction pictures of the prepared samples are analogous to the diffractograms reported earlier for the metal-organic frameworks.<sup>38</sup> In particular, the formation of three crystalline phases with the MIL-53 topology defined as MIL-53(Al)*as*, MIL-53(Al)*ht*, and MIL-53(Al)*lt* was reported. They are stored in the Cambridge Structural Database (CSD) and denoted as SABVOH, SABVUN, and SABWAU, respectively.<sup>39,40</sup>

The analysis of the X-ray powder diffraction patterns of the MIL-53(Al) sample (see Fig. 2) indicates the presence of two crystalline phases in the sample. The main fraction of the sample is represented by the MIL-53(Al) *ht* high-temperature phase with completely open pores of 8.5×8.5 Å. The MIL-53(Al) framework has a rhombic *Imma* structure. The MIL-53(Al)*lt* low-temperature phase is present in small amounts. It has a monoclinic *Cc* symmetry and is characterized by the pore dimensions of 2.6×13.6 Å. The same crystalline phases are identified in the NH<sub>2</sub>-MIL-53(Al) sample (see Fig. 3, a). According to the published data,<sup>31</sup> the ratio of the low-temperature phase to the high-temperature phase (*lt* : *ht*) in the NH<sub>2</sub>-MIL-53(Al) sample can be assessed as 1 : 2.

The X-ray powder diffraction pattern of the NH<sub>2</sub>-MIL-101(Al) sample (see Fig. 3, b) indicates that this matrix crystallizes as the standard *Fd-3m* cubic structure ( $a = 87.95(1)$  Å) in agreement with the published data.<sup>31</sup>

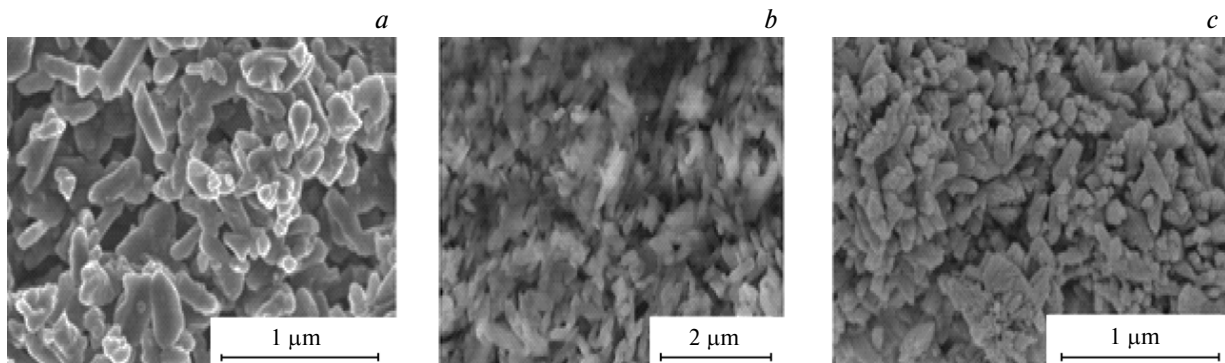


**Fig. 1.** SEM images of samples of MIL-53(Al) (a), NH<sub>2</sub>-MIL-53(Al) (b), and NH<sub>2</sub>-MIL-101(Al) (c).

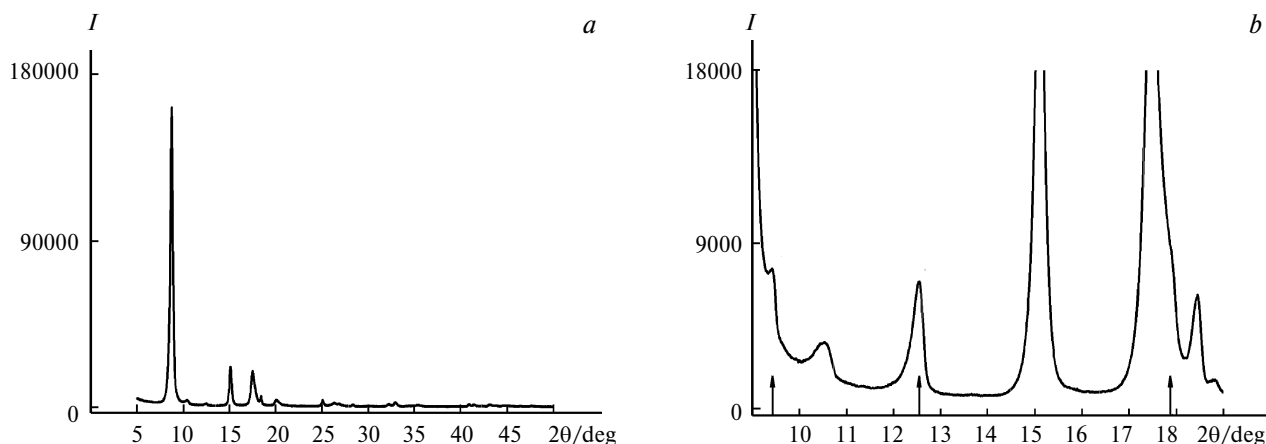


**Fig. 2.** X-ray powder diffraction patterns of the MIL-53(Al) sample for 20 within 5–50° (*a*) and within 9–19° after scaling (S10) (*b*). The vertical arrows indicate positions of first three diffraction reflexes with indices  $hkl = 200$ , 110, and 11-1 for the monoclinic modification of MIL-53(Al)*l*.

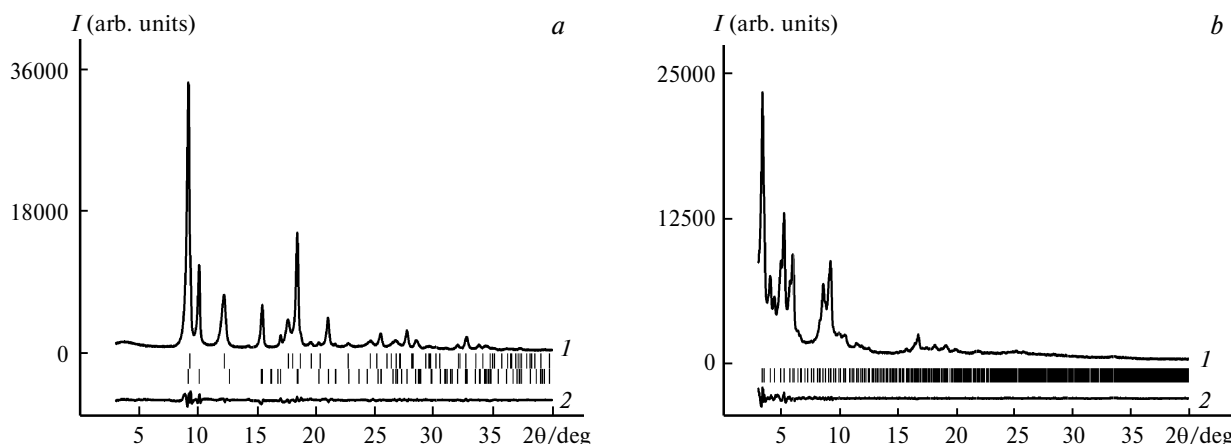


**Fig. 3.** X-ray powder diffraction patterns of the MIL samples (*I*) and the difference curve (*2*) after the Pawley fit:<sup>37</sup> *a* is the NH<sub>2</sub>-MIL-53(Al) two-phase sample; the vertical bars show the calculated reflex positions for two crystalline phases: monoclinic *Cc* phase (upper row) and rhombic *Imma* phase (bottom row); *b* is the NH<sub>2</sub>-MIL-101(Al) monophase sample; the vertical bars show the calculated reflex positions for cubic *Fd-3m* crystalline modification.

Figure 4 shows isotherms of nitrogen adsorption obtained for the samples. Their shapes indicate that the MIL-53(Al) and NH<sub>2</sub>-MIL-53(Al) samples have microporous structure, whereas the NH<sub>2</sub>-MIL-101(Al) matrix contains mesopores.<sup>41,42</sup> Particularly, reversible isotherms of nitrogen adsorption at 77 K and complete filling of pores in the range of very low relative pressures ( $P/P_0 = 0.005$ –0.01) are characteristic of the MIL-53(Al) and NH<sub>2</sub>-MIL-53(Al) samples. As can be seen, the adsorption and desorption branches practically coincide for the MIL-53(Al) adsorbent.

A small hysteresis in the nitrogen adsorption isotherm of the NH<sub>2</sub>-MIL-53(Al) sample corroborates flexibility of the structure of this matrix. The specific surface area ( $S_{BET}$ ) for this sample is equal to ~79 m<sup>2</sup> g<sup>-1</sup> (Table 1) in well agreement with published data.<sup>43</sup> A decrease in the amount of nitrogen adsorbed by NH<sub>2</sub>-MIL-53(Al) in comparison with that adsorbed by MIL-53(Al) can be explained by a difference in the ability of these materials to exhibit the

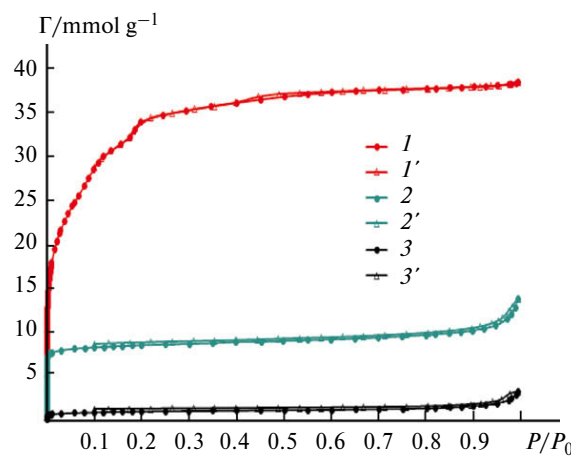


**Fig. 4.** Isotherms of adsorption (1–3) and desorption (1'–3') of nitrogen at 77 K for the MIL samples: NH<sub>2</sub>-MIL-101 (*1*, *1'*), MIL-53(Al) (*2*, *2'*), and NH<sub>2</sub>-MIL-53(Al) (*3*, *3'*).  
Note. Fig. 4 is available in full color on the web page of the journal (<https://link.springer.com/journal/volumesAndIssues/11172>).

**Table 1.** Textural characteristics of the studied adsorbents

Adsorbent	Composition	$S_{\text{BET}}/\text{m}^2 \text{ g}^{-1}$	$V_{\text{tot}}$	$V_{\text{micro}}$	$V_{\text{meso}}$	$r(\text{H}-\text{K})/\text{nm}$
			$\text{cm}^3 \text{ g}^{-1}$			
MIL-53(Al)	AlOHbdc	633	0.479	0.278	0.201	0.7–1.0
NH <sub>2</sub> -MIL-53(Al)	AlOHbdc	79	0.113	0.037	0.076	—
NH <sub>2</sub> -MIL-101(Al)	Al <sub>3</sub> O(abdc) <sub>3</sub>	2895	1.333	1.072	0.261	0.6–0.8
CSAC	CM, —CH <sub>2</sub> —OH, —CH <sub>2</sub> —, —CH=CH—	915	0.472	0.446	0.026	0.9; 1.3
PVC AC-CO <sub>2</sub>	CM, —CH <sub>2</sub> —OH, —CH <sub>2</sub> —, —CH=CH—	733	0.460	0.210	0.250	0.56
PVC AC-Ar-1	CM, (—CH <sub>2</sub> —OH, —CH <sub>2</sub> —)	453	0.657	0.140	0.517	—
PVC AC-Ar-2	CM, —CH <sub>2</sub> —OH, —CH=CH—	393	0.478	0.130	0.348	—
Sibunite	CM, —CH=CH—	372	0.838	0.114	0.724	0.6

Note: CM is carbon matrix;  $S_{\text{BET}}$  is the specific surface area;  $V_{\text{tot}}$  is the total pore volume determined from the adsorption value at relative pressure  $P/P_0 = 0.99$ ;  $V_{\text{micro}}$  is the micropore volume equal to the difference between  $V_{\text{tot}}$  and  $V_{\text{meso}}$ ;  $V_{\text{meso}}$  is the cumulative volume of mesopores calculated from the data for the desorption branch of the isotherm using the Barret–Joyner–Halenda (BJH) procedure for a standard thickness of the adsorption film;  $r(\text{H}-\text{K})$  is the radius of micropore distribution calculated according to the Horvath–Kawazoe method for cylindrical pores (the interaction parameter is equal to  $2.8 \cdot 10^{-43} \text{ erg cm}^4$ ); abdc = 2-amino-benzene-1,4-dicarboxylate, bdc = benzene-1,4-dicarboxylate.

breathing effect. It was found earlier that the structure of NH<sub>2</sub>-MIL-53(Al) at 77 K can correspond to the crystalline phase with very narrow pores.<sup>44</sup>

The branches corresponding to nitrogen adsorption and desorption in the case of the NH<sub>2</sub>-MIL-101(Al) sample form a thin hysteresis loop, which is typical of mesoporous adsorbents. This observation agrees with published data.<sup>45</sup> For this adsorbent, a sharp increase in the amount of nitrogen adsorbed in mesopores is observed at relative pressure values  $P/P_0 \approx 0.2$  (see Fig. 4). As the  $P/P_0$  ratio increases to 1.0, the amount of adsorbed nitrogen gradually increases.

The data on textural characteristics of the prepared samples of the metal–organic frameworks and carbon matrices are shown in Table 1. As can be seen, the specific surface area and geometric parameters of pores of the carbon materials and MIL matrices under study vary in a wide range. The highest specific surface area of almost  $3000 \text{ m}^2 \text{ g}^{-1}$  has the mesoporous NH<sub>2</sub>-MIL-101(Al) framework. The activated carbons practically do not differ in pore size from the microporous MIL-53(Al) framework. In particular, the pore volume and size of the MIL-53(Al) sample almost coincide with the same characteristics obtained for coconut shell activated carbon (CSAC). However, the specific surface area in the case of the carbon matrix is larger than  $S_{\text{BET}}$  of the MIL-53(Al) matrix.

Thus, on the basis of the data of powder X-ray diffraction and low-temperature nitrogen adsorption obtained for the MIL samples, one can conclude that these materials are characterized by phase purity, a high degree of crystallinity, and a well-developed pore system.

**Adsorption on the carbon materials.** According to the data obtained for the adsorption of 2,4-D on the samples of MOFs of the MIL type and on the carbon materials

(Table 2), the highest adsorption capacity is exhibited by microporous carbon materials with large specific surface areas. The pore sizes in these samples (see Table 1) are comparable with the size of the 2,4-D molecule. According to the calculations<sup>46</sup> carried out using the Chem3d Pro program, the cross section of the herbicide molecule is  $\sim 0.21 \text{ nm}$ , whereas its longitudinal section is  $\sim 0.95 \text{ nm}$ .<sup>46</sup> The highest value of the adsorption capacity was shown by the CSAC matrix ( $\sim 383 \text{ mg g}^{-1}$ ).<sup>36</sup> The next adsorption capacity value ( $\sim 293 \text{ mg g}^{-1}$ ) was exhibited by the PVC-CO<sub>2</sub> carbon material, which was prepared by alkaline dehydrochlorination of polyvinyl chloride (PVC) with subsequent activation in CO<sub>2</sub> flow ( $T = 900^\circ\text{C}$ ,  $t = 3 \text{ h}$ , the temperature was increased with a rate of  $5 \text{ deg min}^{-1}$ ).<sup>29</sup> Both of these carbon materials possess a porous structure with a predominance of micropores up to 1 nm in size. A low rate of the herbicide adsorption by carbon matrices from an aqueous solution is typical of adsorbents with micropores with an average diameter of 0.8 nm.<sup>47</sup>

Apparently, the higher adsorption capacity of microporous samples is due to high concentration of the adsorp-

**Table 2.** Adsorption capacity of the adsorbents with respect to 2,4-dichlorophenoxyacetic acid

Adsorbent	Adsorption capacity/mg g <sup>-1</sup>
MIL-53(Al)	336
NH <sub>2</sub> -MIL-53(Al)	241
NH <sub>2</sub> -MIL-101(Al)	172
CSAC	383
PVC AC-CO <sub>2</sub>	293
PVC AC-Ar-1	129
PVC AC-Ar-2	103
Sibunite	159

tion sites.<sup>48</sup> The existence of micropores in the PVC AC-CO<sub>2</sub> can be explained by partial oxidative destruction of the sample in the course of its activation under CO<sub>2</sub>.

To achieve the adsorption equilibrium, about 300 h was needed for samples of carbon materials in which a micropores predominate (Fig. 5, *a*), whereas a shorter time (*ca.* 8–25 h) was required for mesoporous carbon materials. A slow diffusion into slit-shaped pores can be suggested as the limiting step of the adsorption on the microporous carbon matrices. The existence of this type of pores in the studied samples was established on the basis of data on the low-temperature nitrogen adsorption (see Table 1).

Probably, a shorter time required to achieve the adsorption equilibrium in the case of mesoporous carbons is related to a larger size of mesopores, which facilitates the transport of adsorbate molecules to micropores.<sup>7</sup> However, the adsorption capacity of mesoporous carbon matrices is lower than that of microporous carbons (see Table 2). For

instance, the fraction of mesopores is higher for PVC AC-Ar-1 and PVC AC-Ar-2, which were obtained by carbonization of PVC in an argon atmosphere (at different heating rates), than for the sample of PVC AC-CO<sub>2</sub> treated with carbon dioxide. In the PVC AC-CO<sub>2</sub> sample, micro- and mesopores are present in approximately equal ratio (see Table 1). Therefore, a larger volume of mesopores in the case of the PVC AC-Ar-1 sample ensures the accessibility of active adsorption sites, while a larger volume of micropores determines an increase in its adsorption capacity in comparison with PVC AC-Ar-2.<sup>2</sup> Rather low content of functional groups on the surface of the Sibunite sample is apparently responsible for a slower achievement of the adsorption equilibrium as compared to the PVC AC-Ar-1 and PVC AC-Ar-2 samples.<sup>30,49</sup>

It was suggested that the mechanism of the herbicide adsorption on carbon materials includes  $\pi-\pi$ -stacking due to interactions between electron-deficient aromatic ring of 2,4-D and aromatic moieties (benzene rings) on the surfaces of carbon adsorbents.<sup>50</sup> Indeed, IR spectra of Sibunite contain characteristic bands corresponding to the stretching vibrations of C—OH groups of aromatic moieties.<sup>49</sup>

**Adsorption of 2,4-dichlorophenoxyacetic acid on MIL matrices.** The prepared MIL samples are active in the herbicide adsorption. The highest adsorption capacity (~336 mg g<sup>-1</sup>) has the MIL-53(Al) microporous matrix (see Table 2). According to our measurements, pH of the working solution of 2,4-D is equal to 2–3. At this pH value, the herbicide molecules exist in the form of anions, and the highest adsorption capacity of MIL-53(Al) is, probably, related to the electrostatic interaction between herbicide anions and the positively charged framework surface.<sup>25,51</sup>

A decreased adsorption capacity of the NH<sub>2</sub>-MIL-53(Al) matrix relative to its non-modified analog MIL-53(Al) (see Table 2) can be explained by the presence of the amino group in the organic linker of NH<sub>2</sub>-MIL-101(Al), which weakens the breathing effect of the NH<sub>2</sub>-MIL-53(Al) framework in comparison with the MIL-53(Al) framework.<sup>52</sup> In addition, the adsorption capacity of the NH<sub>2</sub>-MIL-53(Al) matrix can be reduced by electrostatic repulsion between the lone electron pairs of the nitrogen atoms of the amino groups of the 2-aminobenzene-1,4-dicarboxylate linkers and the anions of the herbicide molecules.

It is known that a high adsorption activity towards organic compounds in cationic forms exhibited by the NH<sub>2</sub>-MIL-101(Al) matrix is associated with its negatively charged surface. In particular, a high adsorption capacity of this matrix with respect to methylene blue<sup>27</sup> is due to electrostatic interactions between the cations of the adsorbate and lone electron pairs of the amino groups of the organic linker of the framework. Apparently, an analogous effect operates in the case of adsorption of 2,4-D in the form of anions on the NH<sub>2</sub>-MIL-101(Al) matrix.

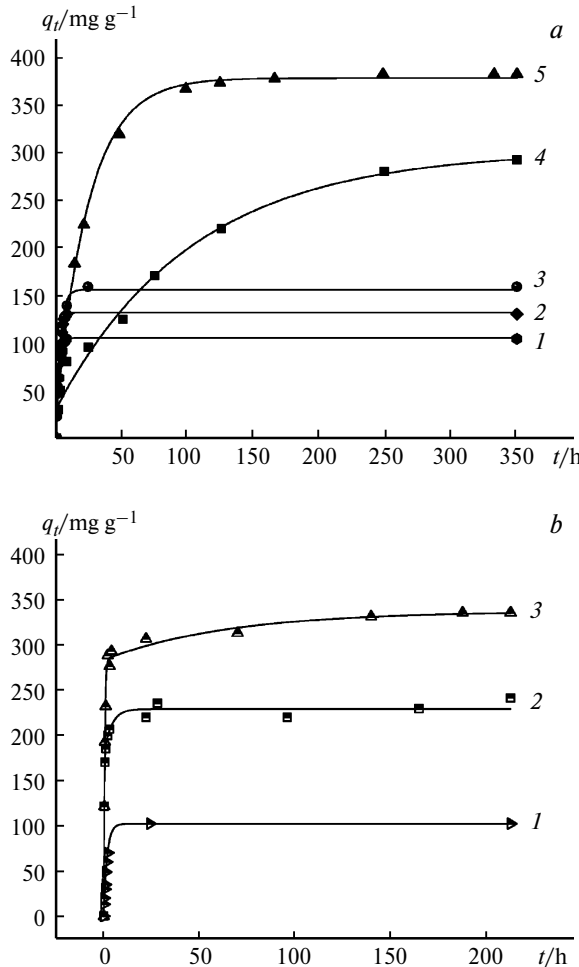


**Fig. 5.** Kinetics of the 2,4-dichlorophenoxyacetic acid adsorption on carbon sorbents (*a*) and MIL samples (*b*); *a*: PVC AC-Ar-2 (1), PVC AC-Ar-1 (2), Sibunite (3), PVC AC-CO<sub>2</sub> (4), CSAC (5); *b*: NH<sub>2</sub>-MIL-101(Al) (1), NH<sub>2</sub>-MIL-53(Al) (2), MIL-53(Al) (3).

In contrast to carbon matrices, the values of the specific surface area of the MIL matrices do not significantly affect the herbicide adsorption. Particularly, the  $\text{NH}_2\text{-MIL-101(Al)}$  mesoporous matrix with a very high specific surface area ( $S_{\text{BET}} = 3000 \text{ m}^2 \text{ g}^{-1}$ ) and wide pores in the forms of mesocavities and entrance windows does not exhibit the breathing effect. According to the data of Table 2, this matrix adsorbs a lower amount of the herbicide than its microporous analog  $\text{NH}_2\text{-MIL-53(Al)}$ . The framework of  $\text{NH}_2\text{-MIL-53(Al)}$  also formed by 2-aminobenzene-1,4-dicarboxylate linkers, has however a lower specific surface area ( $\sim 79 \text{ m}^2 \text{ g}^{-1}$ ). As noted above, this matrix has a pore system in the form of one-dimensional channels and exhibits a pronounced breathing effect, which, possibly, compensates the negative effect of the electrostatic repulsion between 2,4-D anions and amino groups in the organic linker.

A lower adsorption capacity of the  $\text{NH}_2\text{-MIL-101(Al)}$  matrix can be related to its lower stability in the working solution of 2,4-D with pH  $\sim 2$ –3. Indeed, a transformation of the  $\text{NH}_2\text{-MIL-101(Al)}$  sample into a gel-like material was observed when long-term experiments ( $t > 200 \text{ h}$ ) on liquid-phase adsorption were conducted.

The difference in stabilities of micro- and mesoporous MIL matrices in the liquid medium can be explained by specific features of the structure of secondary inorganic building units (SBUs) forming the metal-organic frameworks.<sup>53</sup> In the case of microporous MIL-53(Al) matrix, the  $\text{Al}^{3+}$  ions are shielded from actions of water molecules to a large extent. Indeed, the SBU structures of MIL-53(Al) consist of infinite chains of the  $\text{AlO}_6$  polyhedra, which are connected by benzene-1,4-dicarboxylate anions.<sup>38</sup> On the contrary, SBUs of the  $\text{NH}_2\text{-MIL-101(Al)}$  mesoporous framework are formed by three-dimensional  $\text{Al}_3\text{O}$ -centered clusters, which are interconnected by six molecules of linkers accessible for water molecules.<sup>36</sup>

The analysis of the data of Table 2 shows that the adsorption capacity of the MIL-53(Al) matrix with respect to 2,4-D is somewhat lower than that of the CSAC matrix, but considerably higher (by  $\sim 50 \text{ mg g}^{-1}$ ) than that of the PVC AC-CO<sub>2</sub> sample. In contrast to the case of the CSAC and PVC AC-CO<sub>2</sub> carbon matrices, the adsorption equilibrium ( $q$ ) in the case of investigated MOF samples is achieved faster, for 5–8 h (Fig. 5, b). In the presence of Sibunite and matrices based on PVC, which were obtained by carbonization under an argon atmosphere, the adsorption equilibrium is achieved approximately for the same time ( $\sim 5 \text{ h}$ ) as with the MIL samples.

Thus, we showed that the adsorption processes occurring in the MIL and carbon matrices follow different patterns. The adsorption characteristics of the metal-organic matrices of the MIL type strongly depend on the framework flexibility, topology, and the presence of the amino group in the organic linker, which, in turn, determines the ability of MOF to exhibit the breathing effect.

The most promising matrix for adsorption of 2,4-D and similar compounds is the MIL-53(Al) matrix, which

exhibits considerably more pronounced breathing effect in comparison with its analog  $\text{NH}_2\text{-MIL-53(Al)}$  modified with amino groups. This effect facilitates adsorption of bulky organic molecules by the porous system. The structural and composite characteristics of the MIL-53(Al) matrix at low pH values are favorable for the electrostatic interaction with anions of the 2,4-D herbicide. The stability of this crystalline structure in aqueous medium is also an important factor.

The  $\text{NH}_2\text{-MIL-101(Al)}$  mesoporous matrix is based on the  $\text{Al}_3\text{O}$  secondary building units, whereas the  $\text{NH}_2\text{-MIL-53(Al)}$  microporous framework is formed by the  $\text{AlOH}$  moieties. Therefore, in spite of similar composition of these MOFs, the mesoporous matrix does not exhibit the breathing effect and, in addition, is less stable in aqueous medium than its microporous analog.

Amino groups present in the secondary building units of the  $\text{NH}_2\text{-MIL-101(Al)}$  sorbent function as Brønsted acid sites. These sites create favorable conditions for electrostatic interactions with cationic forms of organic compounds in water, and less favorable for the interactions with anionic forms of compounds, including the herbicide 2,4-dichlorophenoxyacetic acid.

The obtained results can be useful for the development of new adsorbents based on the MOF and carbon matrices and possessing controlled functional characteristics.

This work was performed under financial support of the Russian Foundation for Basic Research (Project No. 18-29-19126).

## References

1. N. A. Khan, Z. Hasan, S. H. Jhung, *J. Hazard. Mater.*, 2013, **244**–**245**, 444; DOI: 10.1016/j.hazmat.2012.11.011.
2. H. Shalla, M. A. Bhat, Z. Yaseen, *J. Environ. Chem. Eng.*, 2018, **6**, 5938; DOI: 10.1016/j.jece.2018.08.063.
3. A. Gupta, R. Zhao, J. T. Novak, C. D. Goldsmith, *Chemosphere*, 2014, **105**, 82, DOI: 10.1016/j.chemosphere.2013.12.066.
4. E. Mohammad-pajoooh, D. Weichgrebe, G. Cuff, *J. Environ.*, 2017, **187**, 354; DOI: 10.1016/j.jenvman.2016.10.061.
5. E. Mohammad-pajoooh, A. E. Turcios, G. Cuf, D. Weichgrebe, K. H. Rosenwinkel, M. D. Vedenyapina, L. R. Sharifullina, *J. Environ. Manag.*, 2018, **228**, 189; DOI: 10.1016/j.jenvman.2018.09.020.
6. L. M. Porto, G. Z. Melgar, M. C. Kasemodel, M. Nitschke, in *Pesticides in the Modern World*, Ed. M. Stoytcheva, Ch. 20, IntechOpen, 2011, p. 407; DOI: 10.5772/17686.
7. V. K. Gupta, B. Gupta, A. Rastogi, S. Agarwal, A. Nayak, *Water Res.*, 2011, **45**, 4047; DOI: 10.1016/j.watres.2011.05.016.
8. M. Ahmaruzzaman, *Energy Fuels*, 2009, **23**, 3, 1494; DOI: 10.1021/ef8002697.
9. C. De Smedt, F. Ferrer, K. Leus, P. Spanoghe, *Adsorpt. Sci. Technol.*, 2015, **33**(5), 457; DOI: 10.1260/0263-6174.33.5.457.
10. A. S. Barreto, A. Aquino, S. C. S. Silva, M. E. de Mesquita, M. J. Calhorda, M. S. Saraiva, S. Navickiene, *Mater. Lett.*, 2011, **65**, 1357; DOI: 10.1016/j.matlet.2011.01.082.

11. L. Joseph, B.-M. Jun, M. Jang, C. M. Park, J. C. Munoz-Sennmache, A. J. Hernandez-Maldonado, A. Heyden, M. Yu, Y. Yoon, *Chem. Eng. J.*, 2019, **369**, 928; DOI: 10.1016/j.cej.2019.03.173.
12. H. S. Cho, J. Yang, X. Gong, Y.-B. Zhang, K. Momma, M. Weckhuysen, H. Deng, J. K. Kang, O. M. Yaghi, O. Terasaki, *Nat. Chem.*, 2019, **11**, 562; DOI: 10.1038/s41557-019-0257-2.
13. M. R. Azhar, H. R. Abid, H. Sun, V. Periasamy, M. O. Tadé, S. Wang, *J. Colloid Interface Sci.*, 2016, **478**, 344; DOI: 10.1016/j.jcis.2016.06.032.
14. C. S. Diercks, M. J. Kalmutzki, N. J. Diercks, O. M. Yaghi, *ACS Cent. Sci.*, 2018, **4**, 1457; DOI: 10.1021/acscentsci.8b00677.
15. A. A. Lysova, R. D. Marchenko, D. G. Samsonenko, A. S. Potapov, V. P. Fedin, *Russ. Chem. Bull.*, 2020, **69**, 1122; DOI: 10.1007/s11172-020-2877-5.
16. A. A. Lysova, D. G. Samsonenko, K. A. Kovalenko, D. N. Dybtsev, V. P. Fedin, *Russ. Chem. Bull.*, 2019, **68**, 793; DOI: 10.1007/s11172-019-2487-2.
17. V. I. Isaeva, L. M. Kustov, *Russ. Chem. Bull.*, 2016, **65**, 2103; DOI: 10.1007/s11172-016-1559-9.
18. B. R. Saifutdinov, M. E. Konnova, V. I. Isaeva, M. M. Il'in, L. M. Kustov, *Russ. Chem. Bull.*, 2017, **66**, 16; DOI: 10.1007/s11172-017-1693-z.
19. M. J. Kalmutzki, N. Hanikel, O. M. Yaghi, *Sci. Adv.*, 2018, **4**; DOI: 10.1126/sciadv.aat9180.
20. S. Dhaka, R. Kumar, A. Deep, M. B. Kurade, S.-W. Ji, B.-H. Jeon, *Coord. Chem. Rev.*, 2019, **380**, 330; DOI: 10.1016/j.ccr.2018.10.003.
21. M. Mon, R. Bruno, J. Ferrando-Soria, D. Armentano, E. Pardo, *J. Mater. Chem. A*, 2018, **6**, 4912; DOI: 10.1039/C8TA00264A.
22. K. Vellingiri, J. E. Szulejko, P. Kumar, E. E. Kwon, K.-H. Kim, A. Deep, D. W. Boukhvalov, R. J. C. Brown, *Sci. Rep.*, 2016, **6**, 27813; DOI: 10.1038/srep27813.
23. H. Saleem, U. Rafique, R. P. Davies, *Micropor. Mesopor. Mater.*, 2016, **221**, 238; DOI: 10.1016/j.micromeso.2015.09.043.
24. X. Li, B. Wang, Y. Cao, S. Zhao, H. Wang, X. Feng, J. Zhou, X. Ma, *ACS Sust. Chem. Eng.*, 2019, **7**, 4548; DOI: 10.1021/acssuschemeng.8b05751.
25. V. I. Isaeva, M. D. Vedenyapina, S. A. Kulaishin, A. A. Lobova, V. V. Chernyshev, G. I. Kapustin, O. P. Tkachenko, V. V. Vergun, D. A. Arkhipov, V. D. Nissenbaum, L. M. Kustov, *Dalton Trans.*, 2019, **48**, 15091; DOI: 10.1039/C9DT03037A.
26. G. Férey, C. Serre, *Chem. Soc. Rev.*, 2009, **38**, 1380; DOI: 10.1039/B804302G.
27. Y. Pi, X. Li, Q. Xia, J. Wu, Y. Li, J. Xiao, Z. Li, *Chem. Eng. J.*, 2018, **337**, 351; DOI: 10.1016/j.cej.2017.12.092.
28. S. A. Kulaishin, M. D. Vedenyapina, L. R. Sharifullina, A. A. Vedenyapin, A. L. Lapidus, *Solid Fuel Chem.*, 2017, **51**, 115; DOI: 10.7868/S0023117720104014.
29. M. D. Vedenyapina, Y. G. Kryazhev, E. A. Raiskaya, S. A. Kulaishin, A. A. Vedenyapin, A. L. Lapidus, *Solid Fuel Chem.*, 2017, **51**, 229; DOI: 10.3103/S0361521917040115.
30. M. D. Vedenyapina, L. R. Sharifullina, S. A. Kulaishin, E. D. Strel'tsova, A. A. Vedenyapin, A. L. Lapidus, *Solid Fuel Chem.*, 2018, **52**, 53; DOI: 10.7868/S0023117718010103.
31. V. I. Isaeva, O. L. Eliseev, R. V. Kazantsev, V. V. Chernyshev, A. L. Tarasov, P. E. Davydov, A. L. Lapidus, L. M. Kustov, *Polyhedron*, 2019, **157**, 389; DOI: 10.1016/j.poly.2018.10.001.
32. V. V. Kachala, L. L. Khemchyan, A. S. Kashin, N. V. Orlov, A. A. Grachev, S. S. Zalesskiy, V. P. Ananikov, *Russ. Chem. Rev.*, 2013, **82**, 648; DOI: 10.1070/RC2013v082n07ABE H004413.
33. F. Salles, H. Jobic, A. Ghoufi, P. L. Llewellyn, C. Serre, S. Bourrelly, G. Férey, G. Maurin, *Angew. Chem., Int. Ed.*, 2009, **48**, 8335; DOI: 10.1002/anie.200902998.
34. P. L. Llewellyn, P. Horcajada, G. Maurin, T. Devic, N. Rosenbach, S. Bourrelly, C. Serre, D. Vincent, S. Loera-Serna, Y. Filinchuk, G. Férey, *J. Am. Chem. Soc.*, 2009, **131**, 13002; DOI: 10.1021/ja902740r.
35. X. Cheng, A. Zhang, K. Hou, M. Liu, Y. Wang, C. Song, G. Zhang, X. Guo, *Dalton Trans.*, 2013, **42**, 13698; DOI: 10.1039/C3DT51322J.
36. P. Serra-Crespo, E. V. Ramos-Fernandez, J. Gascon, F. Kapteijn, *Chem. Mater.*, 2011, **23**, 2565; DOI: 10.1021/cm103644b.
37. G. S. Pawley, *J. Appl. Crystallogr.*, 1981, **14**, 357, DOI: 10.1107/S0021889881009618.
38. C. Li, Z. Xiong, J. Zhang, C. Wu, *J. Chem. Eng. Data*, 2015, **60**, 3414; DOI: 10.1021/acs.jcd.5b00692.
39. T. Loiseau, C. Serre, C. Huguenard, G. Fink, F. Taulelle, M. Henry, T. Bataille, G. Férey, *Chem.—Eur. J.*, 2004, **10**, 1373; DOI: 10.1002/chem.200305413.
40. C. R. Groom, F. H. Allen, *Angew. Chem., Int. Ed.*, 2014, **53**, 662; DOI: 10.1002/anie.201306438.
41. C. M. Granadeiro, A. D. S. Barbosa, S. Ribeiro, I. C. M. S. Santos, B. de Castro, L. Cunha-Silva, S. S. Balula, *Catal. Sci. Technol.*, 2014, **4**, 1416; DOI: 10.1039/c3cy00853c.
42. P. Mishra, H. P. Uppara, B. Mandal, S. Gumma, *Ind. Eng. Chem. Res.*, 2014, **53**, 19757; DOI: 10.1021/ie5006146.
43. C. de Smedt, P. Spanoghe, S. Biswas, K. Leus, P. Van Der Voort, *Adsorption*, 2015, **21**, 243; DOI: 10.1007/s10450-015-9666-8.
44. P. Serra-Crespo, A. Dikhtarenko, E. Stavitski, J. Juan-Alcañiz, F. Kapteijn, F.-X. Coudert, J. Gascon, *CrystEngComm*, 2015, **17**, 276; DOI: 10.1039/C4CE00436A.
45. X. Huang, Q. Hu, L. Gao, Q. Hao, P. Wang, D. Qin, *RSC Adv.*, 2018, **8**, 27623–27630; DOI: 10.1039/c8ra04789h.
46. P. Chingombe, B. Saha, R. J. Wakeman, *J. Colloid Interface Sci.*, 2006, **297**, 434; DOI: 10.1016/j.jcis.2005.10.054.
47. S. A. Kulaishin, M. D. Vedenyapina, L. R. Sharifullina, A. L. Lapidus, *Solid Fuel Chem.*, 2020, **54**, 54; DOI: 10.31857/S0023117720010120.
48. P. Chingombe, B. Saha, R. J. Wakeman, *J. Colloid Interface Sci.*, 2006, **302**, 408; DOI: 10.1016/j.jcis.2006.06.065.
49. O. V. Netskina, E. S. Tauban, A. P. Moisenko, O. V. Komova, S. A. Mukha, V. I. Simagina, *J. Hazardous Mater.*, 2015, **285**, 84; DOI: 10.1016/j.jhazmat.2014.10.017.
50. H. Dolas, O. Sahin, C. Saka, H. Demir, *Chem. Eng. J.*, 2011, **166**, 191; DOI: 10.1016/j.cej.2010.10.061.
51. B. K. Jung, Z. Hasan, S. H. Jhung, *Chem. Eng. J.*, 2013, **234**, 99; DOI: 10.1016/j.cej.2013.08.110.
52. R. Boulé, C. Roland, L. Le Pollés, N. Audebrand, A. Ghoufi, *Nanomater.*, 2018, **8**, 531; DOI: 10.3390/nano8070531.
53. T. Wittmann, R. Siegel, N. Reimer, W. Milius, N. Stock, J. Senker, *Chem.—Eur. J.*, 2014, **21**, 314; DOI: 10.1002/chem.201404654.

Received February 19, 2020;  
in revised form August 12, 2020;  
accepted September 23, 2020